

Lacustrine deposition in response to the middle eocene climate evolution and tectonic activities, Bohai Bay Basin, China

Qing Li^{a,b}, Xuelian You^{c,*}, Zaixing Jiang^d, Shenghe Wu^{a,b}, Dali Yue^{a,b}, Jiangshan Li^{a,b}, Yuan Zhou^{a,b}

^a National Key Laboratory of Petroleum Resources and Engineering, China University of Petroleum (Beijing), Beijing, 102249, China

^b College of Geosciences, China University of Petroleum (Beijing), Beijing, 102249, China

^c School of Ocean Sciences, China University of Geosciences (Beijing), Beijing, 100083, China

^d School of Energy Resources, China University of Geosciences (Beijing), Beijing, 100083, China

ARTICLE INFO

Keywords:

Climate
Eocene
Shahejie formation
Astronomical time scale (ATS)
Bohai bay basin

ABSTRACT

The lower unit of the third member of the Eocene Shahejie Formation (Es_3^l , 42.5 to ~40Ma) is one of the most important petroleum exploration targets in the Bohai Bay Basin. Lacustrine deposits are widely distributed in the Es_3^l unit of the Shulu Sag and display strong vertical and horizontal variations in lithofacies and geochemical characteristics. Based on core data, thin-section petrography, stable $\delta^{13}C$ isotope analyses, and organic geochemistry data, eight lithofacies and six evolutionary lake stages are identified. Combining the results of the astronomical time scale (ATS) and the radiometric age, the correlation between the evolutionary lake stages of Es_3^l and the Eocene global climate curve was illustrated. Tectonic movement caused the basin to subside and resulted in shallow lake formation (Stage 1) during the cooling phase prior to the Middle Eocene Climatic Optimum (MECO); then, the lake level began to rise (Stage 2) with an increasingly warm and humid climate. Stage 3 corresponds to the peak of the MECO and was influenced by the warm and humid climate during the thermal maximum period, forming a deep, freshwater lake. This stage was followed by highly turbulent lake conditions (Stage 4), which were influenced by both the cooling climate and intensive tectonic activity. Subsequently, a stable lake (Stage 5) was formed, which was mainly controlled by the slightly warming climate since the tectonic movement was relatively stable, followed by another stage of turbulent lake conditions (Stage 6). The results show that the global mid-Eocene climate played an important role on the relative lake level changes and TOC enrichment. The MECO led to a rise in the relative sea-level and the obviously rise in relative lake-level in the Bohai Bay Basin. The evolution of the depositional settings was controlled by both global climate and tectonic activities and accounted for the deposition and distribution of lithofacies with distinctly different characteristics and origins.

1. Introduction

Ancient lacustrine sedimentation, an important component of the Earth's sedimentary rock record, is of great significance in reconstruction of paleoclimate and has become important sources or reservoirs of hydrocarbons (e.g., Gierlowski-Kordesch, 1998, 2010; Bohacs et al., 2000; Hao et al., 2011; Grygar et al., 2017; Li et al., 2020a, 2020b). Lacustrine deposits are more sensitive to climate and tectonic changes than marine system deposits due to the relatively small size of the water reservoirs (Goncalves, 2002; Adegoke et al., 2014). Chemical changes in lake water triggered by climate changes commonly result in more varied

sedimentary characteristics within single sequences than those in marine systems (Flügel, 2004; Sarg et al., 2013). Therefore, lacustrine sediments are considered the most valuable archives of information on paleoclimate, clastic sediment supply, base level, and conditions of subsidence during deposition (Tanner, 2010). Studies of lacustrine sedimentary rocks have proven useful in the prediction of oil and gas distribution and in investigations that integrate paleoclimatic and tectonic controls on sedimentation (Carroll and Bohacs, 1999; Tanner, 2010).

Lake deposits commonly show strong vertical and horizontal variations in lithofacies, hydrocarbon potential, and geochemical

* Corresponding author.

E-mail address: youxuelian@cugb.edu.cn (X. You).

<https://doi.org/10.1016/j.marpetgeo.2024.106811>

Received 22 January 2024; Received in revised form 2 March 2024; Accepted 15 March 2024

Available online 23 March 2024

0264-8172/© 2024 Elsevier Ltd. All rights reserved.

characteristics due to sedimentary environment evolution and differences in lake types (Carroll and Bohacs, 2001). Lake type is a major control factor on sedimentary fill pattern, source rock potential, and reservoir properties (Bohacs et al., 2000; Bohacs, 2012; Carroll and Bohacs, 2001). Three categories of ancient lake types can be classified according to the balance between potential accommodation, water and sediment supply: overfilled, balanced-fill, and underfilled lakes (Carroll and Bohacs, 1995, 1999). One lake may commonly evolve from one type to another if the balance between accommodation and water/sediment supply changed (Bohacs et al., 2007; Meléndez et al., 2009; Zhang et al., 2017).

The Bohai Bay Basin is composed of a series of Cenozoic rift lacustrine basins, which are important petroleum-producing plays in China (Hao et al., 2011; Zhao et al., 2014; Li et al., 2014, 2017). The long-term evolution of lake basins in the Bohai Bay Basin has been extensively studied. For example, Hao et al. (2011) discussed the depositional and geochemical variability of the Eocene and Oligocene (spanning nearly 10 million years) lacustrine rift sequences and the environmental evolution of the Bohai Bay Basin. These authors suggested that the lake type evolved from a deep freshwater lake to a shallow saline-alkaline lake and then to a freshwater lake because of changes in tectonic subsidence and climate. However, the long-term changes of lake cannot appropriately reflect the detailed lithofacies variation and the distribution pattern of the lacustrine deposits, which have strong horizontal and vertical heterogeneities (Carroll and Bohacs, 2001). The detailed short-term changes in stratigraphy and knowledge of controls on the

short-term evolution of rift lacustrine basins in the Bohai Bay Basin is still lacking, impeding further exploration.

The Eocene Epoch (~55–34 Ma) was characterized by a dramatic transition in global climate from a warm “greenhouse” to a cool “icehouse” world (Villa et al., 2008). The long-term Eocene cooling trend from the Early Eocene Climate Optimum (EECO) is not entirely monotonic but composed of a series of significant short-term cooling and warming phases (Jovane et al., 2007; Villa et al., 2008). A significant warming anomaly was identified at approximately 41.5 Ma which was designated as the Middle Eocene Climatic Optimum (MECO) and was considered triggered by a transient rise in pCO_2 levels (Zachos et al., 2001, 2008; Jovane et al., 2007; Villa et al., 2008; Galazzo et al., 2013).

The lower unit of the third member of the Eocene Shahejie Formation (Es_3^1 , 42.5 to ~40Ma) is one of the most important source rock intervals and exploration targets in the Bohai Bay Basin (Zhao et al., 2014). The Es_3^1 spans the MECO interval and contains depositional cycles of lacustrine expansion and contraction, which may reflect variations of precipitation and evaporation. However, short-term evolution of depositional processes during rifting and their connection to climate and tectonism are not clear. The Eocene climate and tectonic controls on the lake evolution and formation of organic-rich deposits are still unclear.

The Shulu Sag, one of the most productive oil plays of the Bohai Bay Basin, is a small Eocene half-graben lake basin (Fig. 1), showing strong vertical and horizontal variations in lithofacies and geochemical characteristics during Es_3^1 strata deposition. The Shulu Sag provides a natural laboratory for studying the short-term evolution of the sedimentary

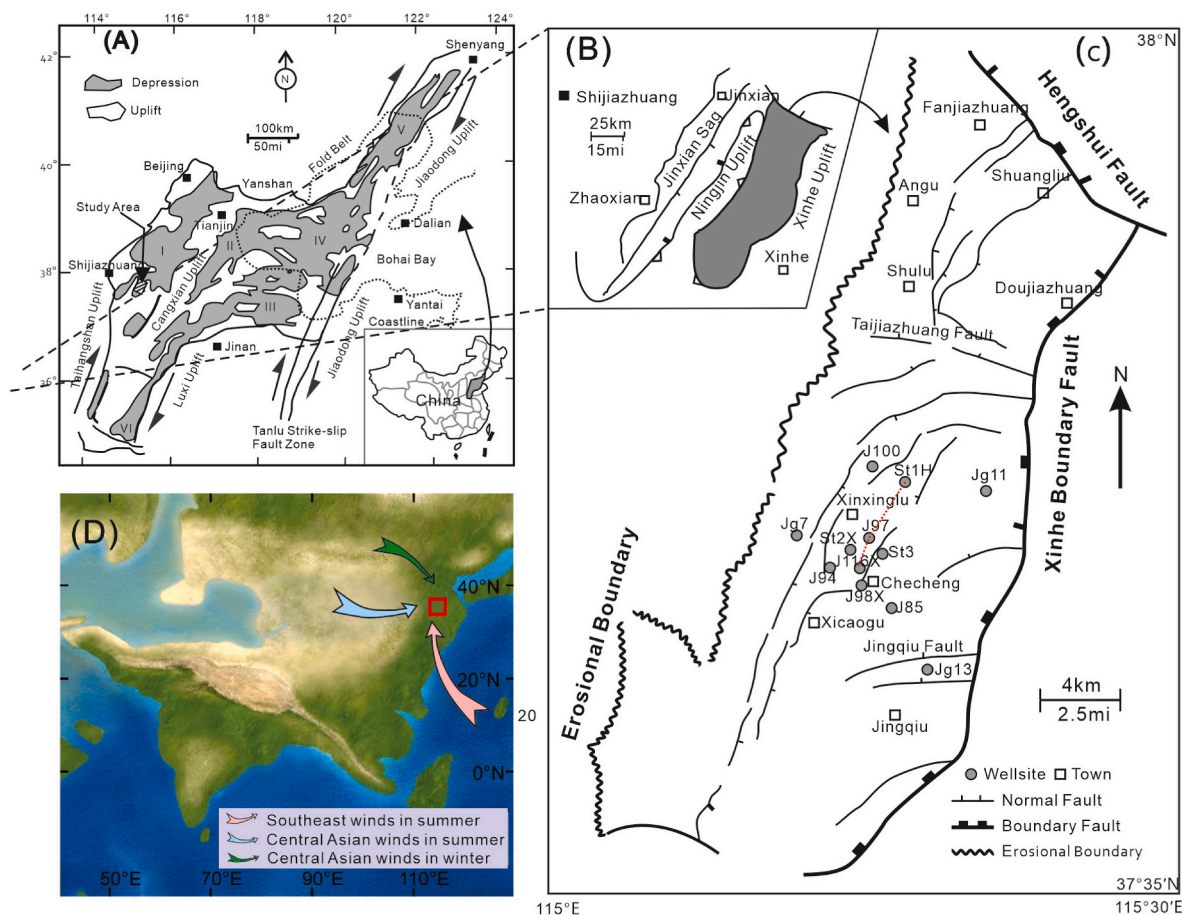


Fig. 1. Location and structural map of the Shulu Sag halfgraben. (A) Tectonic setting of the Shulu Sag halfgraben during the Eocene, located in the southwestern corner of the Jizhong Depression (central Hebei Province) (I). Other subbasins in the Bohai Bay Basin of North China are the Huanghua Depression (II), the Jiyang Depression (III), the Bozhong Depression (IV), the Liaohe Depression (V), and the Dongpu Depression (VI). (B) Sketch of the Shulu Sag. (C) Structural map of the Shulu halfgraben (modified after Jiang et al., 2007). (D) Eocene paleogeography of the Asian mainland showing wind patterns 40 Ma ago (modified after Bougeois et al., 2018). The red square represents study area.

characteristics and depositional setting of a rift lacustrine basin induced by changes in tectonic activities and paleoclimate.

The major objectives of this investigation are to (1) recognize short-term evolutions of the lake basin (the Es₃^L unit of the Shulu Sag), and (2) analysis the Eocene climate and tectonic controls on the lake evolution and formation of organic-rich deposits. The results of this study can help understand the controls on the short-term evolution of rift lakes and clarify lacustrine deposition in response to the Middle Eocene Climatic Optimum (MECO) event and tectonic activities.

2. Geological setting

The Shulu Sag, located in the southern part of the Jizhong Depression, Bohai Bay Basin (Fig. 1A), is a NE-SW trending elongate Cenozoic

half-graben sag bordered by the Xinhe fault to the east, the Ningjin uplift to the west, and the Hengshui fault to the north (Fig. 1B and C). There are two sets of faults in the Shulu Sag that trend nearly W-E and NE-SW. The NE-SW trending faults, mostly active during the Paleogene period. During Es₃^L faults activity was particularly intense (Jin et al., 2008). The other set of faults trending nearly W-E or WNW-ESE, including the Hengshui, Taijiazhuang, and Jinqiu faults (Fig. 1C), formed during the Middle Jurassic to Late Cretaceous Yanshanian Orogeny and controlled the topographic relief within the sag (Yang et al., 2001). The sag was divided into three branches by the W-E trending faults, namely, the northern, middle, and southern parts (Jiang et al., 2007; Zhao et al., 2014). The middle part is the focus of this study.

The Shulu Sag unconformably overlies the Paleozoic (Cambrian-Ordovician and Permian-Carboniferous) basement and is filled with

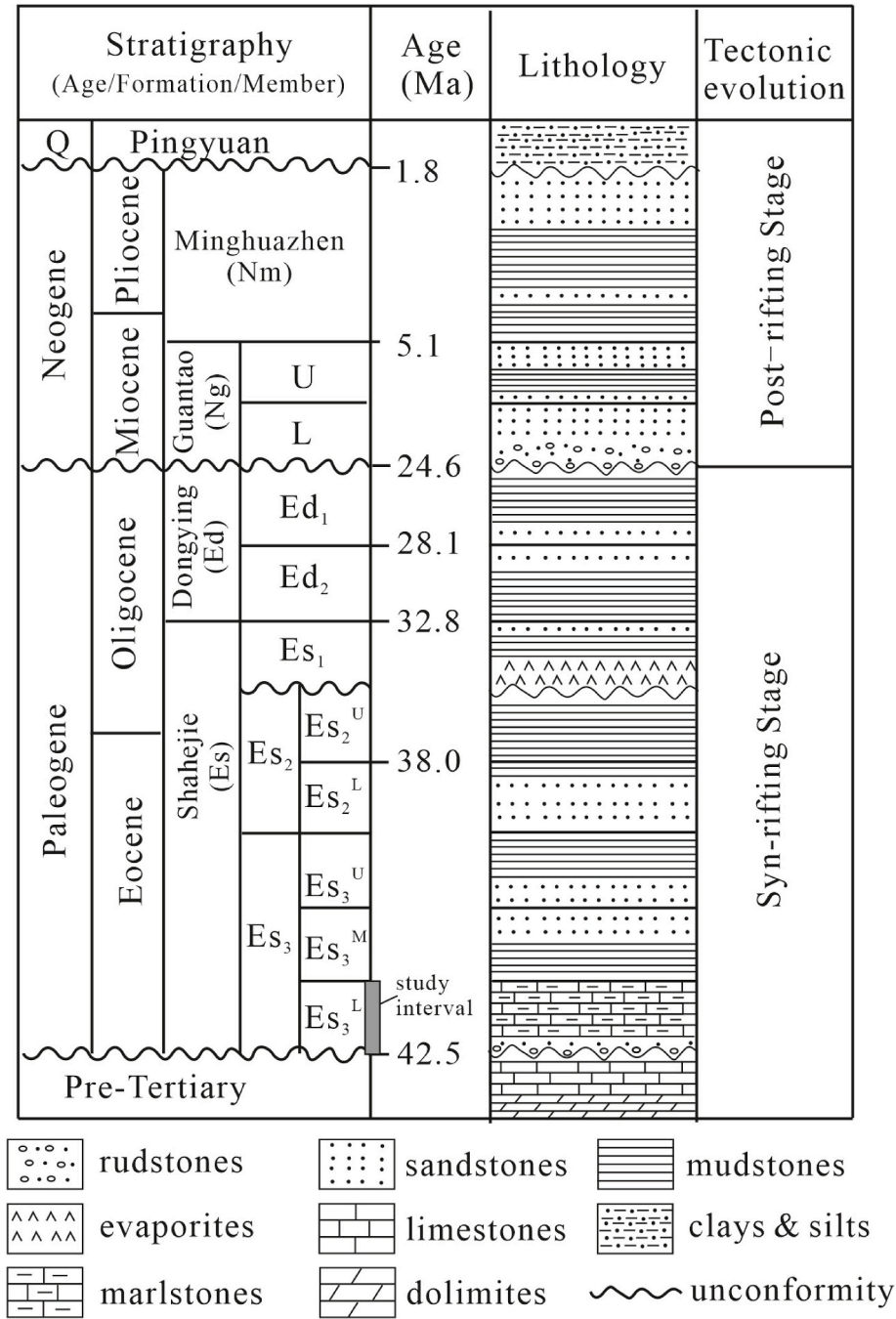


Fig. 2. General Cenozoic stratigraphy of the Shulu Sag, Bohai Bay Basin.

Eocene to Pliocene lacustrine deposits (Li et al., 2017). Five formations deposited in the basin, from bottom to top: the Shahejie, Dongying, Guantao, Minghuazhen, and Pingyuan Formations (Fig. 2). The Shahejie Formation can be further subdivided into three members in the study area, from bottom to top: Shahejie 3 (Es_3), Shahejie 2 (Es_2), and Shahejie 1 (Es_1). The Es_3 consists of three units: the lower unit (Es_3^L), middle unit (Es_3^M), and upper unit (Es_3^U). The Es_3^L base contains gray and light gray clastic carbonates that are overlaid by dark gray marlstone, which is the focus of this study (Fig. 3). During the deposition of the Paleogene, tectonics were active. The synsedimentary faults divided the Shulu Sag into a gentle slope zone, slope break zone, basin plain, and steep slope zone from west to east (Fig. 3). The eastern, southern, and western parts of the Shulu Sag are surrounded by a Mid-Upper Cambrian-Ordovician carbonate bedrock, which was the main source region of the Shulu Sag, providing both clastic and dissolved carbonate (Jiang et al., 2007). The Es_3^L unit can be divided into five sequences from bottom to top: Sequence I, Sequence II, Sequence III, Sequence IV, and Sequence V (Fig. 3; Zheng et al., 2015). In recent years, tight oil has been found in the Es_3^L unit, making the Shulu Sag an important target for tight oil exploration (Zhao et al., 2014; Li et al., 2017).

The paleolatitude and paleogeography of the study area during the Eocene were similar to the present-day. The latitude was approximately between $38^\circ N$ and $38^\circ 35' N$, and the longitude was approximately from $115^\circ E$ to $115^\circ 30' E$ (Fig. 1D; Bougeois et al., 2018). The Asian monsoon system, which controls precipitation over mainland Asia, existed during the Eocene period (Fig. 1D; Liche et al., 2014; Huber and Goldner, 2012; Quan et al., 2012; Wang et al., 2013). Based on micro-paleontology, sporopollen, paleomagnetic stratigraphy, and volcanic rock dating research, the geologic age of begin boundary of the Es_3 in the Bohai Bay Basin is approximately 42.5 Ma and the duration of the Es_3^L is about 2.5 Ma (Hao et al., 2011; Yuan et al., 2015; Wang and Lin, 2012; Wang et al., 2015; Feng et al., 2016).

3. Methods

Cores and cutting samples of the Es_3^L rocks were collected from

exploration wells in the study area. Samples were collected based on detailed core and microscopic observations for total organic carbon (TOC), Rock-Eval pyrolysis, gas chromatography, and gas chromatography-mass spectrometry.

The TOC analysis was determined using a LECO CS-200 carbon analyzer. The hydrogen index (HI) was calculated using the method by Espitalié et al. (1977). Source rock extracts in the study area were treated to isolate saturated hydrocarbon fractions for biomarker analyses. Gas chromatography analysis was performed using an HP-5890, with temperature programmed from $60^\circ C$ to $320^\circ C$ at a rate of $6^\circ C/min$ and then held for 30 min at $320^\circ C$. Gas chromatography-mass spectrometry analysis was performed using a Finnigan Mat SSQ-7000 mass spectrometer with the column oven programmed from $100^\circ C$ to $300^\circ C$ at $4^\circ C/min$. The fragmentograms for steranes (m/z 217) and triterpanes (m/z 191) were recorded and the relative abundances of the triterpanes and steranes were calculated by measuring peak heights.

Natural gamma-ray (GR) logs from well J116X were used for cyclostratigraphic analysis. The data interval for gamma-ray data of well J116X is 0.1 m. Spectral analysis and continuous wavelet analysis were performed to investigate whether the cyclicity records signal is related to astronomical forcing. A band-pass filter was applied to remove very high and low frequency variability. Spectral analysis was performed with the Acycle software (Schulz and Mudelsee, 2002; Li et al., 2019). Wavelet software was provided by Torrence and Compo (1998). The La2010d astronomical model (Laskar et al., 2011) was used to compare with the astronomically GR record.

4. Results

4.1. Heterogeneity of different stratigraphic intervals

Sedimentation in the Es_3^L unit of the Shulu Sag shows a strong heterogeneity. According to the composition, fabric, texture, particle size, and sedimentary structure, 8 lithofacies were recognized in the study area: clast-supported terrigenous carbonate rudstone (CTCR), matrix-supported terrigenous carbonate rudstone (MTCR), mixed-source terrigenous carbonate rudstone (MR), carbonate lithic sandstone (CLS), carbonate lithic siltstone (CLSI), massive marlstone (MM), laminated marlstone (LM), and Fault.

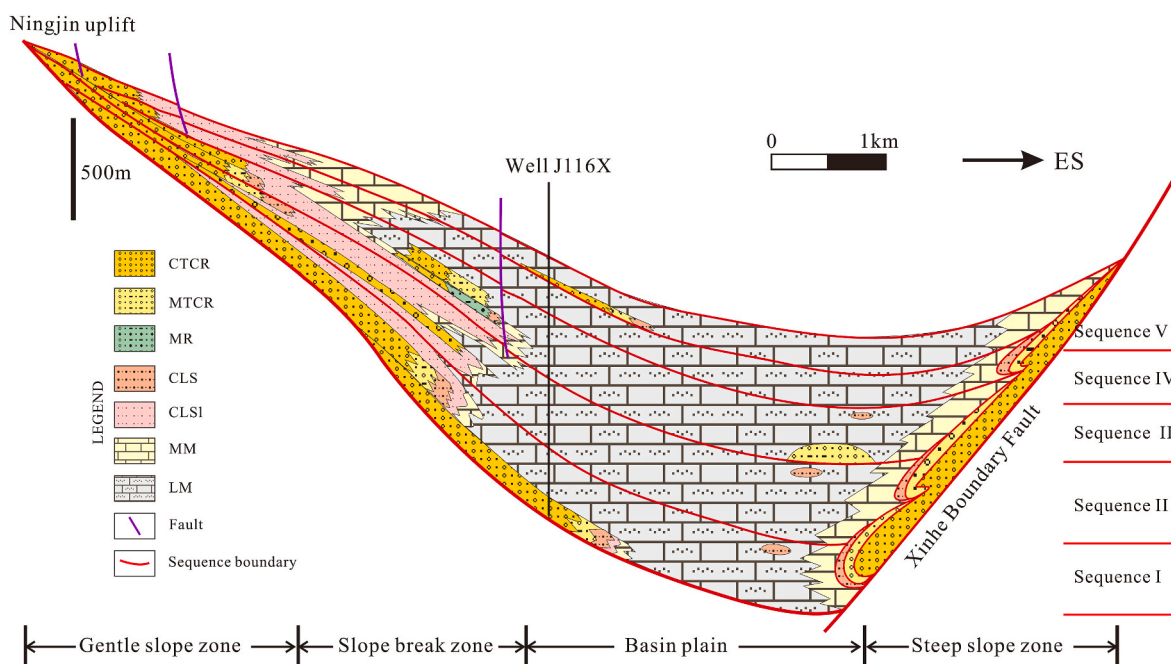


Fig. 3. Transverse section across well St1H in the Es_3^L unit of the Shulu Sag, exhibiting a typical half-graben geometry bounded by the Xinhe fault to the east. The Es_3^L unit can be divided into five sequences: I, II, III, IV, and V from bottom to top (modified after Zheng et al., 2015). CTCR: clast-supported terrigenous carbonate rudstone, MTCR: matrix-supported terrigenous carbonate rudstone, MR: mixed-source terrigenous carbonate rudstone, CLS: carbonate lithic sandstone, CLSI: carbonate lithic siltstone, LM: laminated marlstone, MM: massive marlstone.

rudstone (MR), deformed bedding sandstone (DBS), carbonate lithic sandstone (CLS), carbonate lithic siltstone (CLSI), massive marlstone (MM), and laminated marlstone (LM) (Figs. 4 and 5). The CTCR is mainly composed of carbonate breccias and sand-grade carbonate debris as interstitial materials. The MTCR has a high matrix content, enclosing terrigenous gravels and forming matrix-supported rudstone. The MR contains two types of coarse-grains: extrabasinal and intrabasinal gravel. DBS commonly has wavy/convoluted bedding. CLSI commonly shows massive, plane-parallel, and normally graded bedding, with local plane-parallel bedding. The MM is homogeneous without laminar structures, containing micrite marl, some organic matter, and a small amount of silt-sized terrigenous grains and ostracod debris. LM is dark-colored and is composed of regular to irregular laminae. The LM is commonly rich in organic matter. The thickness of laminae is generally less than 1 mm. The LM Es₃¹ is mainly composed of dark gray laminated marlstone (LM).

The cross section (Well J116X - Well J97 - Well St1H) shows that the variation trends of the facies association and organic geochemical characteristics of the sedimentation in the Es₃¹ unit of the Shulu Sag are similar (Fig. 6). In order to analyze vertical evolutions in depositional environments, the Es₃¹ can be divided into 6 intervals on the basis of the variation trends of the facies association and the organic geochemical characteristics (Fig. 6). The characteristics of the different intervals are described below.

Interval 1: This interval is mainly composed of terrigenous carbonate rudstone, with low TOC content (0.07 wt% to 0.21 wt%, with an average of 0.13 wt%, Fig. 6) and low hydrogen index (HI) values (39–229 mg HC/g TOC, with an average of 151 mg HC/g TOC, Fig. 7). The plot of HI vs T_{max} shows that the organic matter type is mainly type III (Fig. 7). The Pr/Ph ratio is less than 1 (between 0.33 and 0.55, with an average of 0.47). The $n\text{-C}_{21}/n\text{-C}_{22}$ ratio is relatively low (between 0.51 and 1.27, with an average of 0.88). The gammacerane/C₃₁ hopane ratio is relatively high (0.38–0.66, with an average of 0.50) (Fig. 8). The Pr/n-C₁₇ ratio ranges from 0.44 to 0.56 (average of 0.52) and the Ph/n-C₁₈ ratio ranges from 0.76 to 1.48 (average of 1.09).

Interval 2: The abundance of terrigenous carbonate rudstone decrease in this stage, and marlstone increases. Interval 2 displays TOC contents of 1.11 wt%–2.35 wt% (average of 1.4 wt%, Fig. 6) and HI

values of 304–561 mg HC/g TOC (average of 390 mg HC/g TOC) (Fig. 7). The values of TOC and HI generally increase in this interval. The organic matter type is mainly type II to types II–III (Fig. 7). Stage 2 has Pr/Ph ratios ranging from 0.51 to 0.74 (average of 0.65), $n\text{-C}_{21}/n\text{-C}_{22}$ ratios from 0.75 to 1.52 (average of 1.06), and gammacerane/C₃₁ hopane ratios from 0.12 to 0.41 (average of 0.28) (Fig. 8). The Pr/n-C₁₇ ratio and Ph/n-C₁₈ ratio range from 0.44 to 0.60 (average of 0.51) and from 0.63 to 0.86 (average of 0.79), respectively.

Interval 3: A large set of organic-rich marlstone developed in interval 3. The lithofacies is composed of laminated marlstone, interbedded with minor massive marlstone, and terrigenous carbonate rudstone. This interval has TOC contents ranging from 1.29 to 4.92 wt% (average of 2.46 wt%) and HI values from 438 to 659 mg HC/g TOC (average of 540.5 mg HC/g TOC) (Fig. 7). The average TOC and HI values of this stage are higher than those of the other stages. The Pr/Ph ratio is mainly less than 1 (between 0.58 and 1.08, with an average of 0.81). The $n\text{-C}_{21}/n\text{-C}_{22}$ ratio is high (between 0.72 and 1.64, with an average of 1.03). The gammacerane/C₃₁ hopane ratio is low (0.09–0.17, with an average of 0.12) (Fig. 8). The Pr/n-C₁₇ ratio ranges from 0.45 to 0.75 (average of 0.57), and the Ph/n-C₁₈ ratio ranges from 0.56 to 1.19 (average of 0.79).

Interval 4: Interval 4 is mainly composed of marlstone, terrigenous carbonate rudstone, and carbonate lithic sandstone. Rudstones are more abundant than in interval 3. This interval has TOC contents ranging from 1.16 to 3.52 wt% (average of 2.02 wt%) and HI values from 285 to 631 mg HC/g TOC (average of 510.4 mg HC/g TOC) (Fig. 7). The contents of TOC and TS in interval 4 are less than those of stage 3. The Pr/Ph ratio is highly variable from 0.50 to 2.17, with an average of 1.39. The $n\text{-C}_{21}/n\text{-C}_{22}$ ratio is low, ranging from 0.44 to 1.72, with an average of 0.85. The gammacerane/C₃₁ hopane ratio also shows abnormal fluctuations (from 0.05 to 0.77, with an average of 0.24), indicating that the lake was more turbulent at this stage (Fig. 8). The Pr/n-C₁₇ ratio ranges from 0.44 to 0.94 (average of 0.68), and the Ph/n-C₁₈ ratio ranges from 0.30 to 0.88 (average of 0.61).

Interval 5: Interval 5 is mainly composed of laminated marlstone, with a small amount of rudstone and carbonate lithic sandstone. Compared to interval 4, the distribution of rudstone decreases, and









Lithofacies	Sketch	Characterization	Sedimentary origin
LM		LM is dark-colored and is composed of regular to irregular laminae	Seasonal laminae or muddy trubidites
MM		The MM is homogeneous without laminar structures	Turbid clouds triggered by earthquakes
CLSI		CLSI commonly developed massive bedding and normally graded bedding, with local plane-parallel bedding	Turbidity currents
CLS		CLS commonly has massive bedding and normally graded bedding, with local plane-parallel bedding	Sand debris flow to turbidity currents
DBS		DBS commonly has wavy/convoluted bedding	Hydroplastic deformation caused by earthquakes
MR		There are two types of gravels in MR: terrigenous gravel and intrabasinal gravel.	Sandy debris flows within a sublacustrine setting
MTCR		The MTCR has a high matrix content. Gravels are contained in the matrix, forming matrix-supported rudstone	Slide and slump in subaqueous fans
CTCR		The CTCR is mainly composed of carbonate breccias and sand-grade carbonate debris as interstitial materials	Slide and slump in subaqueous fans

Fig. 4. Characterization and sedimentary origin of lithofacies in the Shulu sag. CTCR: clast-supported terrigenous carbonate rudstone, MTCR: matrix-supported terrigenous carbonate rudstone, MR: mixed-source rudstone, DBS: deformed bedding sandstone, CLS: carbonate lithic sandstone, CLSI: carbonate lithic siltstone, MM: massive marlstone, LM: laminated marlstone.

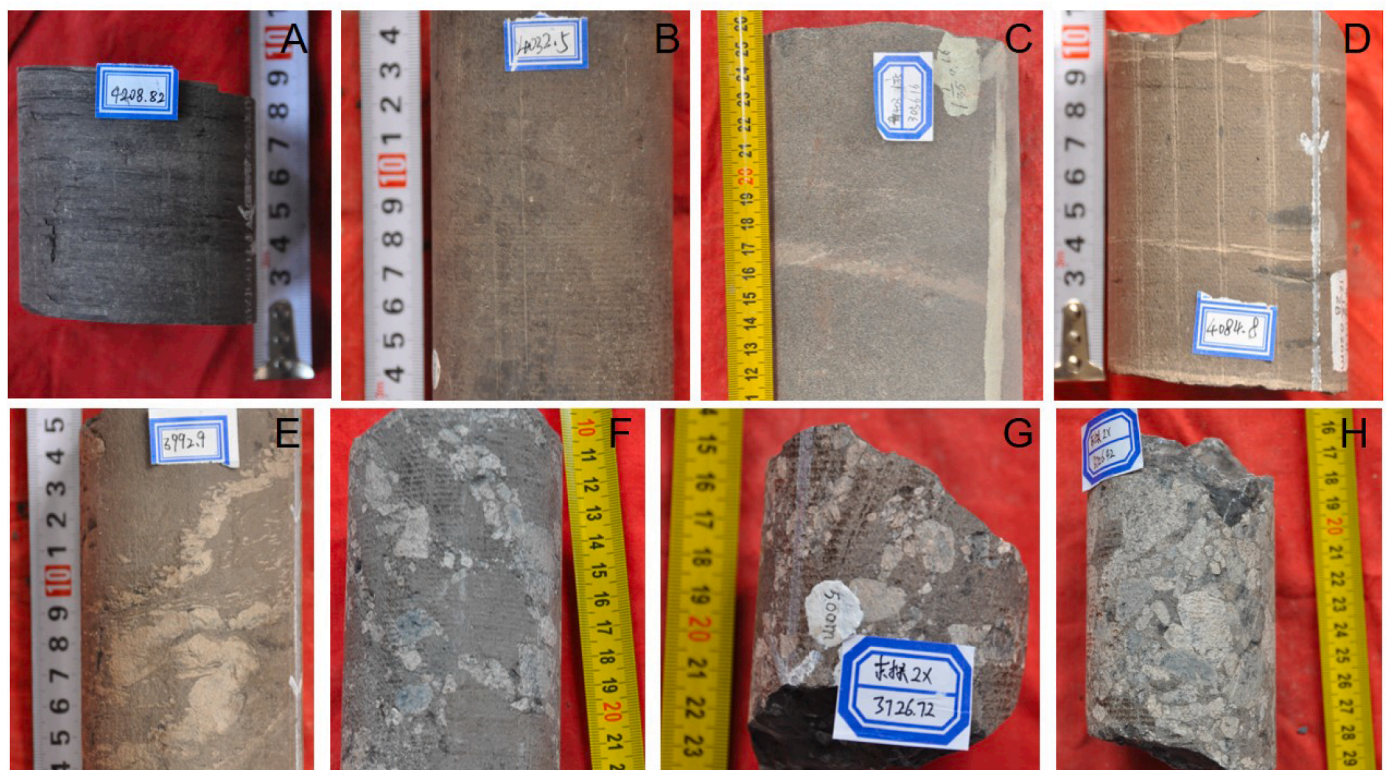


Fig. 5. Photographs of cores showing the characteristics of different lithofacies within the Es₃^I unit. (A) Dark-colored laminated marlstone. Well St1H, 4208.82 m. (B) Dark-colored massive marlstone. Well St1H, 4032.5 m. (C) carbonate lithic siltstone. Well J403, 3056.16 m. (D) carbonate lithic sandstone, Well St1H, 4084.8 m. (E) deformed bedding sandstone. Well St1H, 3992.9 m. (F) mixed-source rudstone. Well St2X, 3729 m. (G) matrix-supported terrigenous carbonate rudstone. Well St2X, 3726.72 m. (H) clast-supported terrigenous carbonate rudstone. Well St2X, 3726.42 m.

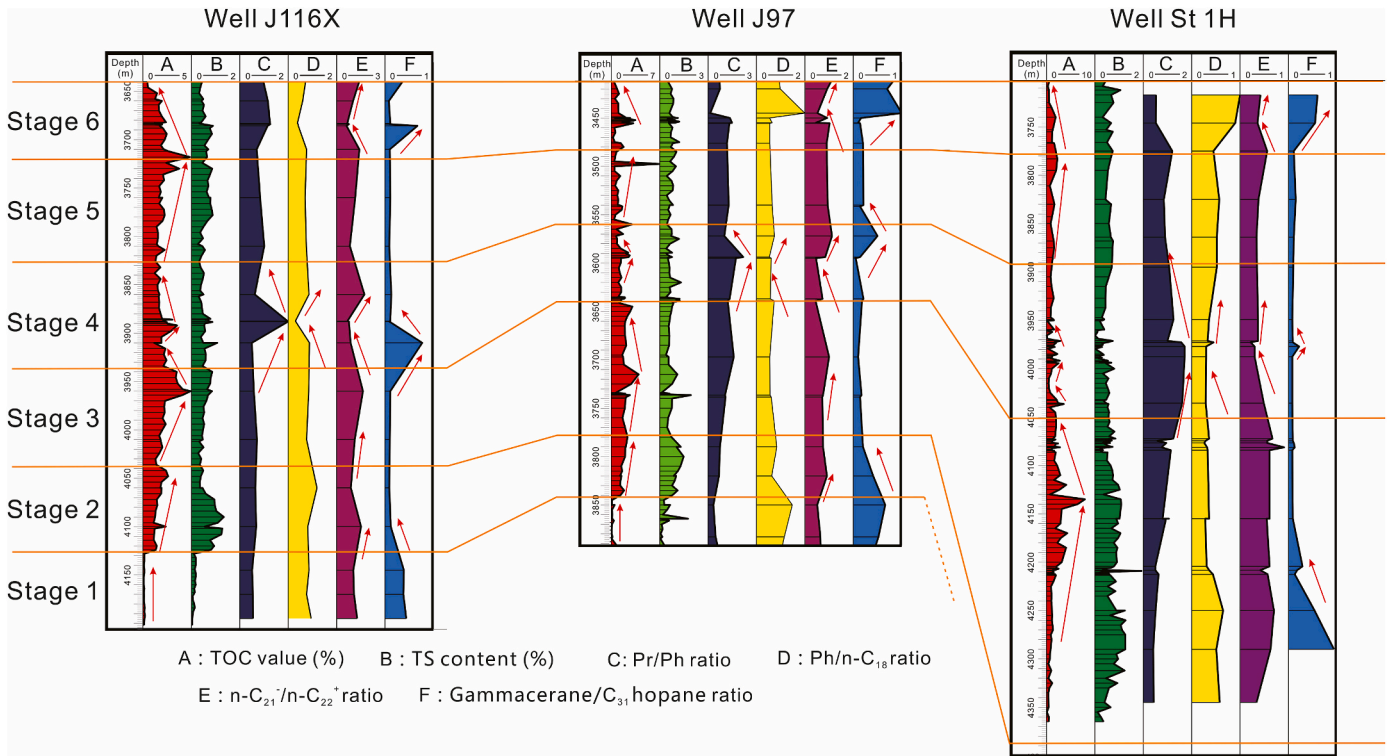


Fig. 6. Correlation of organic geochemical characteristics for wells J116X-J97-St1H (see Fig. 1 for location).

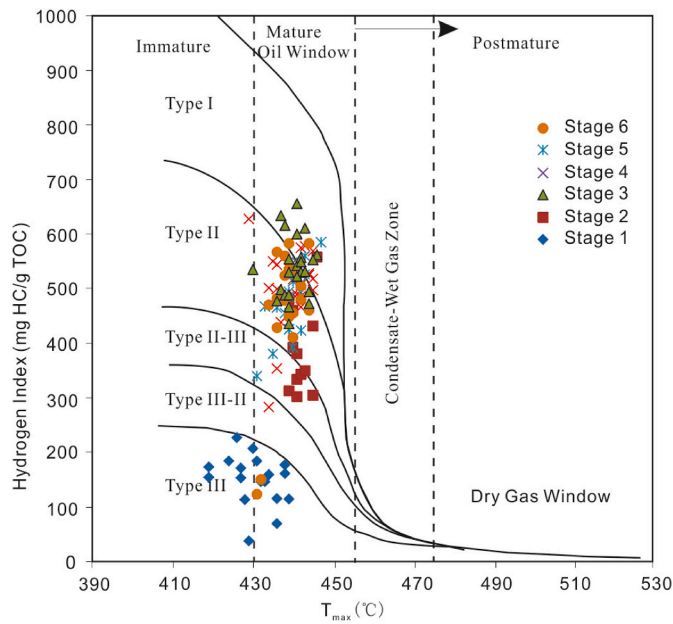


Fig. 7. Plot of the hydrogen index (HI) versus pyrolysis temperature of the maximum yield of pyrolysate (T_{max}) for the Es_1 rock, showing the kerogen type and the thermal stages (boundary lines modified after Mukhopadhyay et al., 1995).

marlstone becomes the predominate lithofacies. This interval has TOC contents ranging from 1.38 to 3.75 wt% (average of 1.93 wt%), and HI values from 342 to 588 mg HC/g TOC (average of 477.3 mg HC/g TOC) (Fig. 7). The contents of TOC and TS increase overall. The Pr/Ph ratio ranges from 0.84 to 1.27, with an average of 1.04. The ratio of $n-C_{21}/n-C_{22}^+$ increases (from 0.83 to 1.16, with an average of 0.98). The gammacerane/ C_{31} hopane ratio is low and stable (from 0.09 to 0.21, with an

average of 0.14) (Fig. 8). The values of the Pr/ $n-C_{17}$ and Ph/ $n-C_{18}$ ratios tend to be stable, ranging from 0.52 to 0.84 (average of 0.70) and from 0.65 to 0.75 (average of 0.70), respectively.

Interval 6: Interval 6 is mainly composed of marlstone, interbedded with terrigenous carbonate rudstone and carbonate lithic sandstone. The values of TOC, HI, and sulfur decrease. This interval has TOC contents ranging from 0.44 to 4.84 wt% (average of 1.86 wt%) and HI values from 125 to 586 mg HC/g TOC (average of 464.6 mg HC/g TOC) (Fig. 7). The Pr/Ph ratio has a large fluctuation again, from 0.70 to 1.48, with an average of 1.16. The $n-C_{21}/n-C_{22}^+$ ratio is low, ranging from 0.45 to 1.41, with an average of 0.87. The gammacerane/ C_{31} ratio is also abnormal (from 0.08 to 0.70, with an average of 0.24), indicating that the lake was turbulent again at this stage (Fig. 8). The Pr/ $n-C_{17}$ ratio ranges from 0.45 to 0.86, with an average of 0.57, and the Ph/ $n-C_{18}$ ratio ranges from 0.38 to 0.98, with an average of 0.58.

4.2. Cyclostratigraphy

To better understand the control of global climate on local sedimentation, establishing a high-precision chronostratigraphic framework is fundamental. The radiometric ages and paleontological data have been widely used to determine the absolute ages of strata. Because of the limited data and insufficient continuity of radiometric ages and paleontological data, the astronomical time scale (ATS) has been widely applied to defining and correlating the chronostratigraphic framework in recent years (e.g. Fiet et al., 2006; Mitchell et al., 2008; Hinnov and Ogg, 2007; Wu et al., 2009). Lacustrine depositions in continental rift basins are particularly suitable for high-resolution cyclostratigraphic studies and for establishing astronomical time scales, because of their sensitivity to changes in climate and tectonic (Olsen and Kent, 1999; Prokoph and Agterberg, 2000; Hinnov, 2004). The classical Milankovitch theory indicates that Earth orbital parameters include eccentricity, obliquity, and precession. The changes in these parameters can induce variations in the insolation received on the Earth surface, resulting in

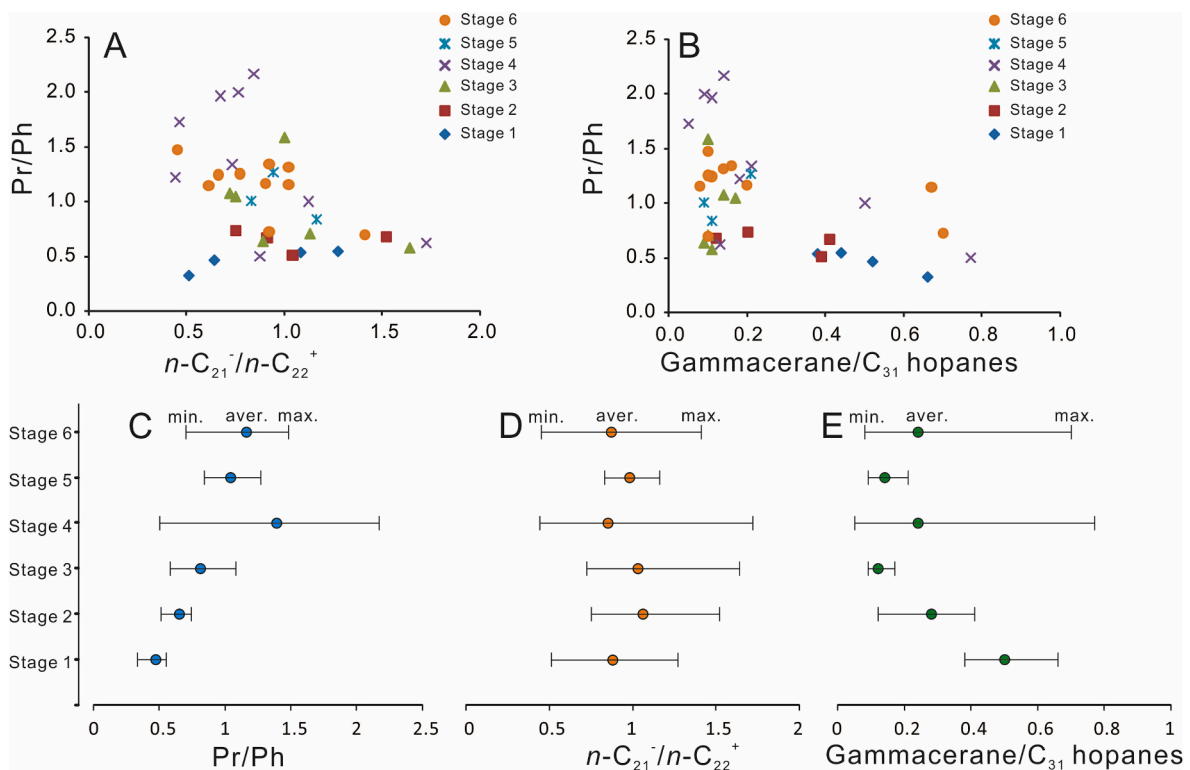


Fig. 8. Biomarker characteristics of the Es_1 unit. (A) Plot of the pristane/phytane ratio (Pr/Ph) versus $n-C_{21}/n-C_{22}^+$. (B) Plot of the Pr/Ph versus gammacerane/ C_{31} hopanes. (C) Pr/Ph ratio of each stage. (D) $n-C_{21}/n-C_{22}^+$ ratio of each stage. (E) Gammacerane/ C_{31} hopanes ratio of each stage.

periodic changes of climate and sediments (Milankovitch, 1941; Laskar et al., 2004).

The location of the Shulu sag in Eocene was similar to the present-day geographic position around 38°N and 115°E. According to Laskar et al. (2004), an insolation curve at 38°N and 115°E from 42.5 to 40 Ma was calculated (Fig. 9A). Four distinct frequency bands are revealed from the continuous wavelet analysis scalogram (Fig. 9B). The spectral analysis result shows the principal eccentricity periods of 405 ka (E_3), 125.05 ka (E_2) and 96.19 ka (E_1), principal obliquity periods of 39.7 ka (O_1) with lesser ones of 51.04 ka (O_2) and 29.08, and principal precession periods of 23.16 ka (P_2), 21.94 ka, 18.66 ka (P_1), and 16.24 ka (Fig. 9C). These periods are referred to as the Es_3^I “canonical” orbital variations in this study.

The gamma-ray logging curves can reflect continuous vertical changes of clay and organic materials content in sediments which are

sensitive to climate changes (e.g., Serra, 1984; Hinnov, 2004), and hence have been widely used for cyclostratigraphic analysis (Wu et al., 2009). The well J116X is mainly composed of marlstone and the geological record of this well appears to be continuous without any hiatus. Therefore, in this study, natural gamma-ray log of well J116X penetrating the Es_3^I was selected for the cyclostratigraphic analysis. The data interval for gamma-ray data of well J116X is 0.1m. Detailed wavelet analysis and spectral analysis were conducted on the natural gamma-ray logging of the Es_3^I from the well J116X.

Wavelet analysis of gamma-ray reveal relatively continuous cycles with periods of ~100m, 20.0–27.5m, 8.8–11.1m, 4.1–5.5m, which have high wavelet coefficients (Fig. 9D). To identify whether the observed cycles in sedimentary strata were controlled by astronomical forcing, the most commonly way is to compare the relative ratio of the observed cycles with that of the Milankovitch cycles (Hinnov, 2000; Weedon,

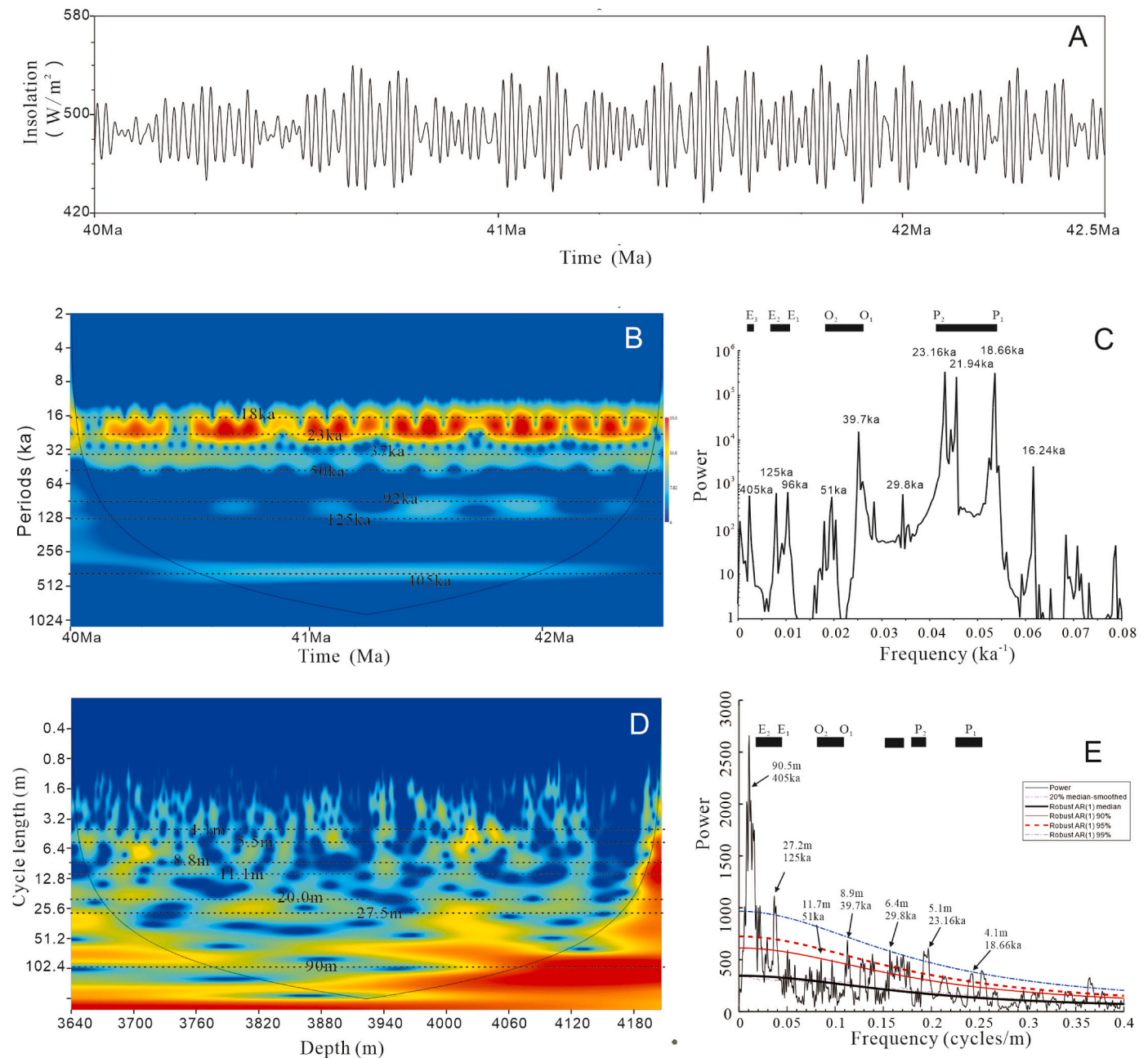


Fig. 9. (A) Insolation curve at 38°N and 115°E from 42.5 to 40 Ma. (B) Wavelet scalogram of the theoretical insolation curve. (C) Spectral analysis of the theoretical insolation curve. (D) Wavelet scalogram of the gamma-ray logging of well J116X. (E) Spectral analysis of the gamma-ray logging of well J116X

2003; Wu et al., 2009). The Milankovitch cyclicities are approximately 405 ka: 100 ka:40 ka:20 ka (long eccentricity, short eccentricity, obliquity, precession). The ratios of the major periods found in the natural gamma-ray (90.5m, 20.0–27.5m, 8.8–11.1m, 4.1–5.5m) approximates 20:5:2:1, which matches well with the Milankovitch cyclicities. Spectral analysis of the gamma-ray logging reveals six main peaks of these cycles and the ratio for the six main peaks is 90.5m: 27.2m:11.7m: 8.9m: 6.4m: 5.1m (corresponding to 405: 125: 51: 39.7: 29.8: 23.16: 18.66) (Fig. 9E). These ratios are similar to the results of spectral analysis of insolation curve at 38°N and 115°E from 42.5 to 40 Ma (Fig. 9C). Thus, the sedimentary cyclicity in well J116X is considered to be formed by orbital forcing (Weedon, 2003). The major periods 90.5m, 20.0–27.5m, 8.8–11.1m, 4.1–5.5m were formed most likely by long and short eccentricity, obliquity and precession, respectively. The eccentricity cycles (405 ka and 125 ka), which shows stable and clear signals, were used to construct the ATS (Figs. 9 and 10). Gaussian band-pass filter was used to filter the signals of the long eccentricity and short eccentricity cycles (405 kyr and 125 kyr). The filtering outputs of the gamma-ray logging are shown in Fig. 10. Counting from the base of the Es3L, every cycle is numbered. A total of 21.6 short eccentricity cycles were counted. The established ATS from well J116X indicates that the duration of the Es3L is 2.7 Ma.

5. Discussion

5.1. Depositional setting evolution

The depositional environment of Es₃^I in the Shulu Sag has been discussed based on petrological characteristics in the literature (e.g., Jiang et al., 2007). There is a lack of studies on the characteristics and controlling factors of deposition in small-scale phases of the lake evolution during Es₃^I deposition, integrating lithofacies and organic geochemical indicators. The organic geochemical characteristic profile of well J116X-well J97-well St1H shows that the organic geochemical index of these three wells has similar trends (Fig. 6). The organic geochemical index can reflect the sedimentary environment and the water chemistry (Peters et al., 2005). The similar trends for the organic geochemical evolution in different wells in the study area suggest that the sedimentary environments in the study area experienced a similar evolutionary process.

Lithofacies is a distinctive rock type that forms under certain conditions of sedimentation and different lithofacies characteristics and assemblages can reflect depositional conditions, terrigenous supply, and characteristics of lake-level change (e.g., Sarg et al., 2013; Hickey and Bo, 2007). TOC content depends not only on the lake's original productivity but also on the preservation conditions. The original productivity is closely related to the paleoclimate and nutrients. In addition,

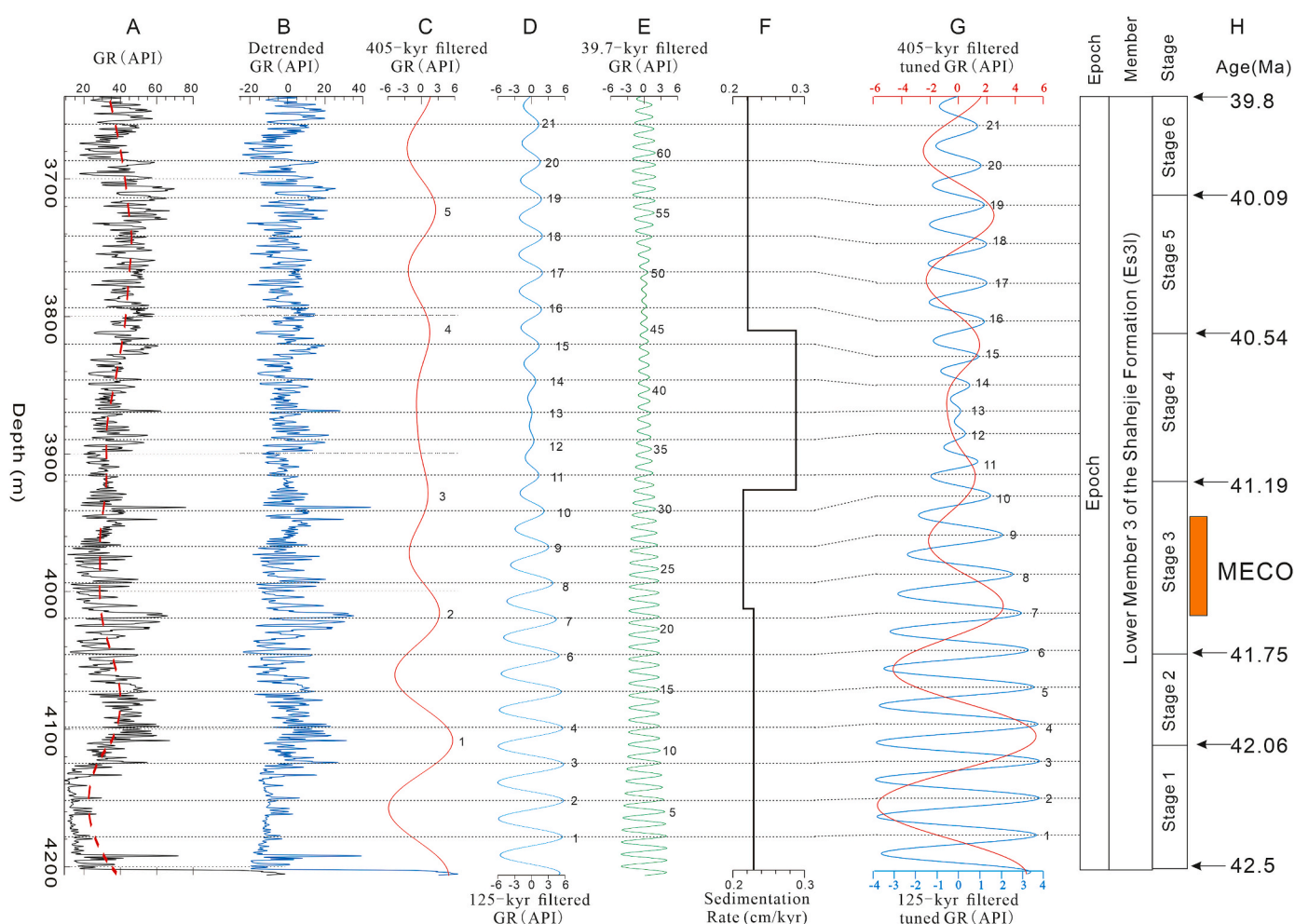


Fig. 10. Astronomical time scale (ATS) for the Es₃^I of Well J116X in the Dongying Depression. (A) The gamma-ray logging of well J116X (3694–4200 m). (B) The detrended gamma-ray logging of well J116X (3694–4200 m). (C) ~90.5 m filtered cycles (405-kyr filtered) in the Es₃^I (D) ~27.2 m filtered cycles (125-kyr filtered) in the Es₃^I (E) ~8.9 m filtered cycles (39.7-kyr filtered) in the Es₃^I (F) The sedimentation rate curve is calculated based on ~405-kyr tuning of the statistically significant cycles. (G) The long eccentricity and short eccentricity filtered cycles of the Tuned GR series. (H) The ages for boundaries of each stage according to Astronomical time scale (ATS).

preservation condition is related to the water depth and physical and chemical conditions of the water body. Therefore, TOC content can indicate ancient water depths, climates, and water conditions (e.g. Abouelresh and Slatt, 2012; Rein and Negendank, 1993). Sulfur is present in the Es_3^1 sedimentary rocks mainly as framboidal pyrite. Total sulfur (TS) content can indicate the water depth and nature of the water body, and high TS content commonly implies an anoxic environment (Ogawa et al., 2009). The Pr/Ph ratio is commonly used as an indicator of the redox conditions and salinity of depositional environments during sedimentation and diagenesis (Peters et al., 2005), because archae-bacteria, which are important sources of phytane (Chen et al., 1996), are commonly confined in specific ecological environments, typically hypersaline environment (Tissot and Welte, 1984). A low Pr/Ph ratio (<1.0) usually indicates anoxic and hypersaline environments (Hossain et al., 2009; Chen et al., 1996), and a high Pr/Ph ratio (>3.0) indicates freshwater with inputs of terrigenous materials under a suboxic-oxic environment or corresponds to coal-bearing sediments (Ten Haven et al., 1987; Chen et al., 1996). The isoprenoids to n -alkanes (such as Ph/ n - C_{18}) ratio can be used to indicate the source of organic matter, redox conditions, and maturation (Ficken et al., 2000). The distributions of n -alkanes are widely used to determine the source of organic matter (Duan and Ma, 2001; Mohialdeen et al., 2015). Aquatic organisms are rich in lipid compounds and contain high amounts of low-molecular weight n -alkanes. On the other hand, terrestrial plants have high amounts of large-molecular weight n -alkanes (Peters et al., 2005; Hou, 2011). Therefore, the ratio of the n -alkanes that have less carbon than C_{21} to the n -alkanes that have more carbon than C_{22} (ratio of n - C_{21}/n - C_{22}^+) can indicate the proportion of lower aquatic organisms (such as plankton and algae) in organic matter. Gammacerane is a kind of C_{30} -triterpane, which is commonly associated with high-salinity depositional environments. The different ratios of gammacerane to C_{31} hopane can reflect the change in water salinity (Liang et al., 2017; Hao et al., 2011).

According to the changes in the organic geochemical index, combined with the variety of vertical lithofacies, the depositional environments of each stage and the evolution of the depositional environments during Es_3^1 deposition in the Shulu Sag are discussed.

5.1.1. Stage 1: shallow brackish lake

This stage was the initial development of the lake basin and is mainly composed of CTCR and MTCR, which have a wide range of distribution from the edge of the lake basin to the slope break zone, indicating high terrigenous inputs. The TOC and TS contents of the sediments at this stage are very low, reflecting that the lake level was low at this period. The Pr/Ph ratio is less than 1, indicating that the sediments formed in an anoxic environment. The ratio of n - C_{21}/n - C_{22}^+ is relatively low, and the organic matter type is mainly terrestrial type III, indicating the algae productivity is low and the organic matter source primarily contains terrestrial plants with minor amounts of algae. The ratio of gammacerane/ C_{31} hopane is relatively high, indicating that the salinity of the lake water was relatively high at this time. The presence of calcretes in the rudstone of Stage 1 and the absence of evaporative minerals (Jiang et al., 2007) suggest that the climate during this interval is neither too dry nor too humid but an intermediate climate (Platt and Wright, 1992).

During Stage 1, the lake level was generally low, the input of terrestrial materials was high, the abundance of organic matter and the productivity of algae low, the depositional water body under oxygen-deficient conditions, the salinity was relatively high, and the climate was intermediate (Fig. 10).

5.1.2. Stage 2: rising lake

In Stage 2, the distribution range of rudstone decreased, and marlstone began to develop. This interval is mainly composed of LM interbedded by CTCR and MTCR, indicating that the terrestrial input decreased. The TOC and TS content increased, suggesting lake-level rise. The Pr/Ph ratio is less than 1, indicating that the environment was

anoxic. The ratio of n - C_{21}/n - C_{22}^+ increased, and the type of organic matter became mainly type II-III and type II, reflecting that the proportion of low algae began to increase. The ratio of gammacerane/ C_{31} hopane decreased, indicating that the salinity of the lake decreased.

In general, during this stage, the lake level rose, the input of terrestrial material decreased, the abundance of organic matter and the algae productivity increased, the depositional water body was anoxic, and the salinity was low (Fig. 10).

5.1.3. Stage 3: deep, freshwater lake

Large sets of organic-rich marlstones developed in Stage 3. The widely distributed LM suggest the water bodies were stratified. The TOC content is highest among all the stages, and the TS content is high, indicating that the lake level was high and the terrestrial input was low. The Pr/Ph ratio is less than 1, indicating that the depositional environment is anoxic. The ratio of n - C_{21}/n - C_{22}^+ is high, and the organic matter type is mainly type I and type II, indicating that the productivity of algae is high, and algae is the main source of organic matter. The ratio of gammacerane/ C_{31} hopane is low, indicating low salinity of the lake water at this interval.

Therefore, during Stage 3, the lake level was high, the water body was quiet and stratified, the input of terrestrial material was low, the abundance of organic matter and the productivity of algae was high, the depositional water body was anoxic, and the salinity was low (Fig. 10).

5.1.4. Stage 4: highly turbulent lake

The lithofacies of Stage 4 are composed of LM, MM, CTCR, MTCR, and CLS. Rudstones in Stage 4 are more abundant than in Stage 3, but less than in Stage 1. Stage 4 sedimentary rocks contain evidence of extensive soft-sediment deformation structures (Fig. 5E), which have been interpreted as seismites formed in a slump fan by debris flows induced by earthquakes (Zheng et al., 2015).

The TOC content decreases, and the TS content is low, indicating that the lake level declined. The Pr/Ph ratio largely varies, indicating the instability of the redox environment. The low ratios of Ph/ n - C_{18} and n - C_{21}/n - C_{22}^+ and the appearance of type III organic matter indicate a decrease in algae and the input of abundant terrigenous materials. The ratio of gammacerane/ C_{31} hopane also appeared abnormal. These variable organic geochemical characteristics indicate that the lake was highly turbulent.

Thus, during this stage, the lake level decreased, the input of terrestrial materials increased, the abundance of organic matter and the algae productivity decreased, the redox conditions and salinity of the depositional water fluctuated, and the lake was highly turbulent (Fig. 10).

5.1.5. Stage 5: stable lake

Stage 5 consists mainly of LM and a small amount of rudstones. Compared to Stage 4, the distribution range of rudstones decreased, and marlstones became the main lithofacies. The content of TOC and TS increased in general, indicating that the lake level rose and the input of terrestrial materials decreased. The value of the Pr/Ph ratio is slightly less than 1, indicating that the sediments were formed under an oxygen-deficient environment. The organic matter type is mainly type II. The value of the Ph/ n - C_{18} ratio remained stable, and the ratio of n - C_{21}/n - C_{22}^+ increased, indicating that the proportion of algae was higher in Stage 5 than in Stage 4. The ratio of gammacerane/ C_{31} hopane has a low value and is stable, indicating that the salinity of the lake was relatively low.

During Stage 5, the lake level increased, the input of terrestrial materials decreased, the abundance of organic matter and the productivity of algae increased, the water body was oxygen-deficient, the salinity was low, and the water body was stable (Fig. 10).

5.1.6. Stage 6: turbulent lake

Stage 6 is mainly composed of LM, MM, CTCR, MTCR, and CLS. The content of TOC and TS decreased, indicating that the lake level fell, and

the input of terrestrial materials increased. The Pr/Ph ratio has large fluctuations again, indicating that the redox environment was complex and variable. The organic matter type includes both type II and type III kerogen. The low ratios of Ph/ n -C₁₈ and n -C₂₁/ n -C₂₂ indicate that the algae content decreased, while the land plant content increased, indicating a large amount of terrigenous material input. The ratio of gammacerane/C₃₁ hopane also appeared abnormal, indicating that the lake was relatively turbulent again in this stage.

In general, during the depositional period of Stage 6, the lake level decreased, the input of terrestrial materials increased, the abundance of organic matter and the productivity of algae decreased, the redox conditions and salinity of the depositional water fluctuated, and the lake was turbulent again (Fig. 10).

The deposits of the different lake stages are the products of deposition during different periods of evolution of the basin. The lake evolution from shallow (Stage 1) to rising (Stage 2), to deep, freshwater lake (Stage 3) indicates an overall trend of deepening with time (Fig. 10). The deep lake was then followed by highly turbulent lake conditions (Stage 4), indicating a trend of shallowing and a stage with active tectonics. The following stable lake (Stage 5) and turbulent lake (Stage 6) show another deepening-shallowing trend.

5.2. Correlation between the eocene global climate curve and the lake stages

Combining the results of ATS and the radiometric age, the Es₃¹ in the study area was dated from 42.5Ma to 39.8 Ma, and the ages for boundaries of each stage were established (Fig. 10). And the correlation between the evolutionary lake stages of Es₃¹ in the Shulu Sag and the global climate reconstruction by Zachos et al. (2001, 2008) during the middle Eocene was illustrated (Fig. 11). Stage 3 corresponds to the peak of the MECO (Figs. 11 and 12).

After the Early Eocene Climate Optimum (EECO), the middle Eocene experienced an overall trend of cooling (Fig. 12A). However, during the period between 42 Ma and 41 Ma, the temperature fluctuated and increased dramatically at approximately 41.5Ma, forming the Middle Eocene Climatic Optimum (MECO) (Fig. 12B), which lasted between 350 and 650 kyr (Zachos et al., 2001, 2008; Galazzo et al., 2013).

According to the correlation (Fig. 12B and C), it is suggested that Stage 1 formed during the cooling phase before the MECO. During Stage 2, the global temperature began to increase. Stage 3 corresponds to the MECO period. Stage 4 suggest a cooling climate with less humid conditions, which coincide well with the cooling part of the Eocene climate curve. Stage 5 and stage 6 experienced a warming and cooling global climate respectively.

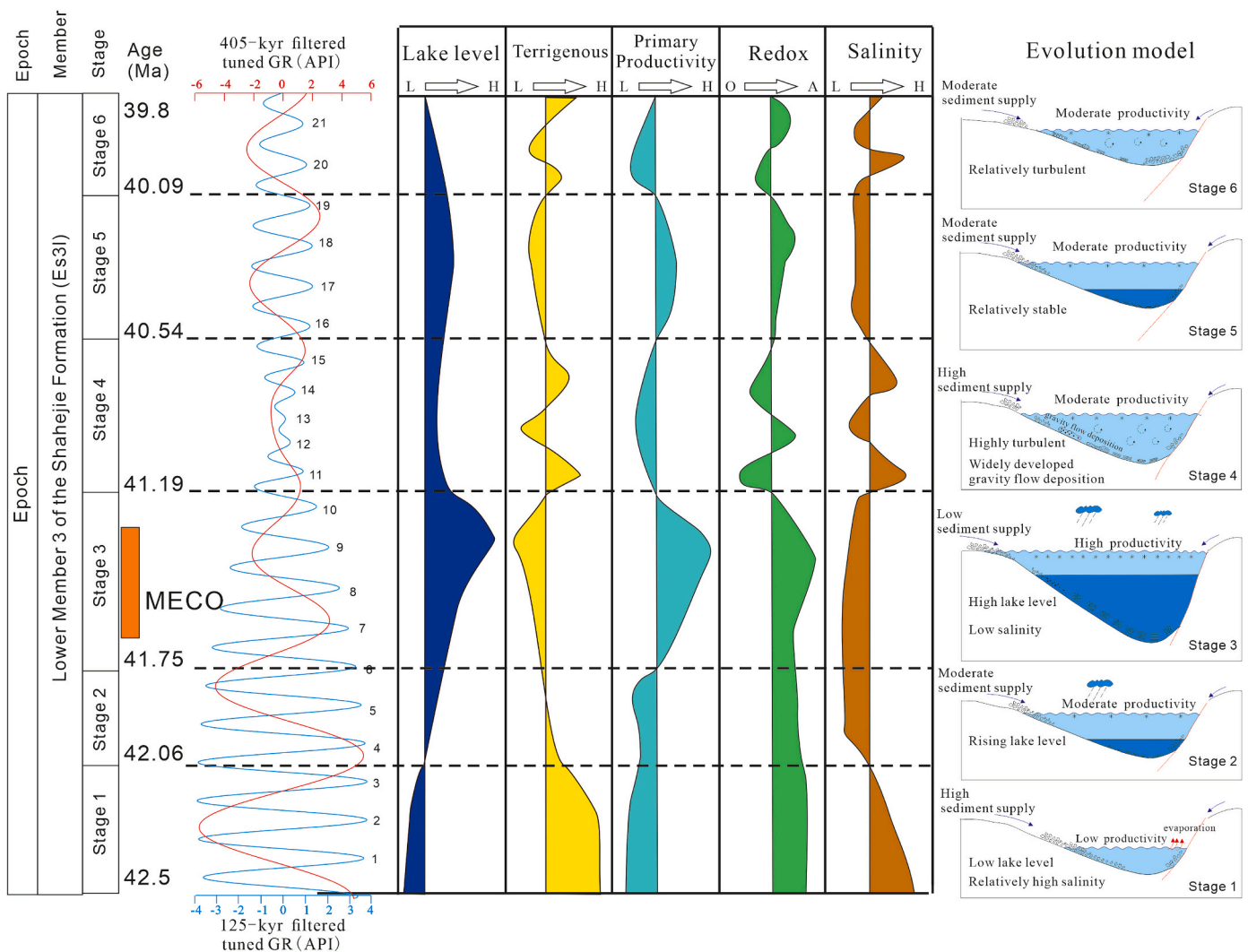


Fig. 11. Evolution model of the sedimentary environment of the Es₃ unit. "L" means low, "H" means high, "O" means oxidizing, "A" means anoxic.

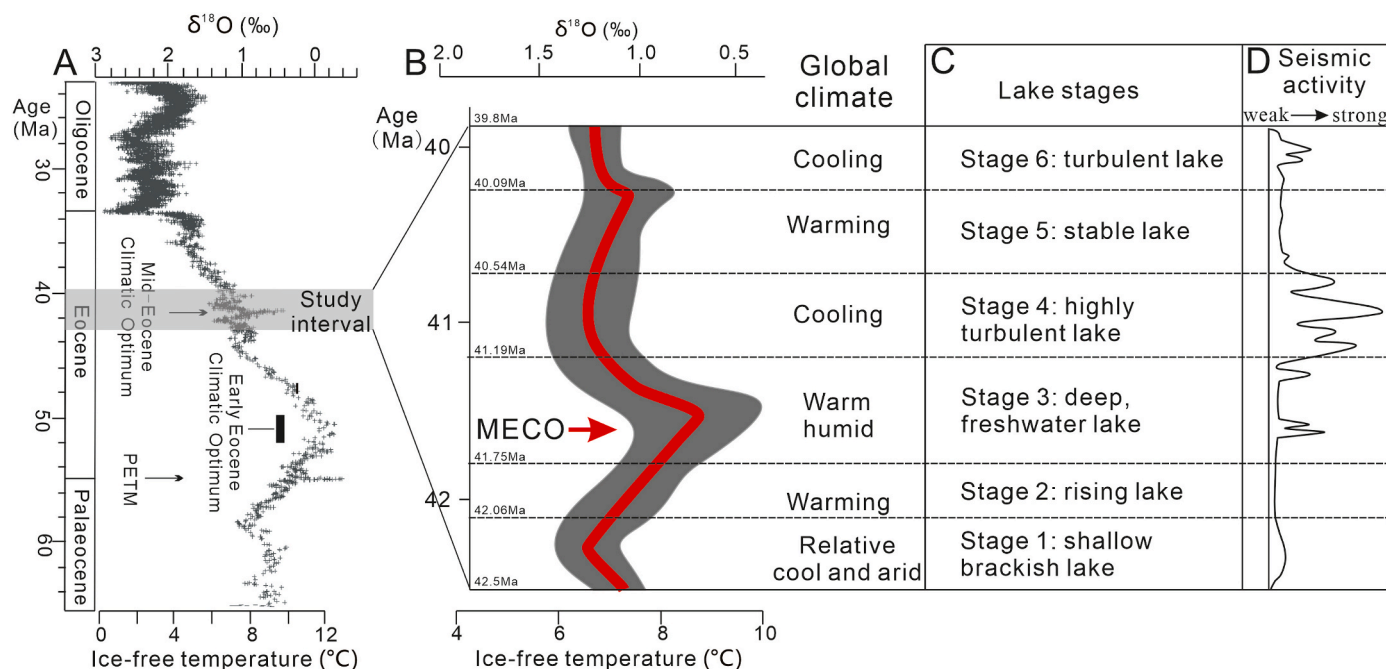


Fig. 12. Correlation between the Eocene global climate curve and evolutionary lake stages in this study. (A) Cenozoic global climate trends (modified after Zachos et al., 2001, 2008). (B) Eocene global climate curve (modified after Zachos et al., 2001, 2008). (C) Lake stages of the Es_3^1 unit in the study area. (D) Seismic activity of the study area (modified after Zheng et al., 2015).

5.3. Control factors on depositional processes

According to the correlation, it is suggested that Stage 1 formed during the cooling phase before the MECO (Fig. 12 B and C). The relatively high-salinity lake water and appearance of calcretes indicate that the climate was relatively cool and arid during this period. Stage 1 also coincides with the first occurrence of seismic indicators (Zheng et al., 2015, Fig. 12D) that might point to the beginning of tectonic activity. During Stage 1, which is the beginning of lake evolution, tectonic movement caused the subsidence of the basin and resulted in lake formation.

During Stage 2, the global temperature began to increase (Fig. 12B and C). The increasing lake level and algae productivity and decreasing salinity indicate a change from a relatively cool and arid climate to a slightly wetter period with rainfall runoff. The Stage 2 deposits indicate an upward trend of lake deepening. Since the seismic activity in Stage 2 was weak (Fig. 12D), the deposition was mainly controlled by an increasingly warm and humid climate.

Stage 3 corresponds to the peak of the MECO (Figs. 11 and 12). The high lake level with high organic matter content and widespread organic-rich marlstone deposits during Stage 3 suggest that the warm climate was probably accompanied by more humid conditions. Although the climate during Stage 3 was warm and humid, the terrigenous input was low. This was probably due to the stabilizing effect of vegetation which was dense during the warm and humid climatic condition (Jiang et al., 2007). Some studies indicate that the periodic changes of Earth's orbit could lead to MECO event and lead to the melting or expansion of continental ice sheets, resulting in relatively sea-level rise (Rohl et al., 2004). According to ATS, the lake-level of the Shulu sag showed gradually rising during the MECO from ~41.6 to 41.2 Ma (Figs. 11 and 12). The interpretations of lake-level variation in the Dongying Depression and Dongpu Depression in the Bohai Bay Basin also showed the same trend. Thus, the MECO led to relative sea-level rise and also obviously rise in relative lake-level in the Bohai Bay Basin. Seismic activity in Stage 3 began to increase because of increased stress (Zheng et al., 2015, Fig. 12 D), leading to accelerated subsidence. Thus, the deposition in Stage 3 was mainly influenced by the warm and humid

climate during the thermal maximum period and accompanied by the tectonic activity, resulting in a deep, freshwater lake.

The high terrigenous input into the lake and decrease in TOC value and distribution range of organic-rich marlstone during stage 4 suggest a cooling climate with less humid conditions, which coincide well with the cooling part of the Eocene climate curve (Fig. 12 B and C). Stage 4 is also the period with the most intense tectonic activity (Zheng et al., 2015, Fig. 12 D). Intensive tectonic movement during Stage 4 was thought to trigger gravity flows, resulting in widely developed seismites and gravity flow deposition (Zheng et al., 2015). The Stage 4 deposition was influenced by both the cooling climate and intensive tectonic activity, resulting in a highly turbulent lake.

Stage 5 reflects an increase in runoff and lake level (Fig. 11). Stage 5, stable lake, was mainly controlled by the slightly warming climate since the tectonic movement was relatively stable (Fig. 12). Stage 6 suggests another stage of turbulent lake condition (Fig. 10), which were less intense than those in Stage 4. Stage 6 was influenced by both the cooling climate and tectonic activity (Fig. 12).

The results show that the deposition in the Es_3^1 unit was influenced by both tectonics and climate changes. The depositional changes were obviously affected by global climate changes during the mid-Eocene, because climate can influence overall runoff, nutrient transport, terrigenous input, etc. (Tănăsescu-Milkevičienė and Sarg, 2012). In addition, tectonic activities affect terrigenous inputs and depositional processes.

The Middle Eocene had enhanced greenhouse conditions and high atmospheric CO_2 content (pCO_2) (Pagani et al., 2005; Zachos et al., 2001). The enhanced greenhouse conditions of Middle Eocene might have higher atmospheric water vapor loading and a reinforced hydrological cycle (Prell and Kutzbach, 1992; Huber and Goldner, 2012). Along with the globally warm condition, the global climate was high humidity and had enhanced monsoon precipitation and strong continental weathering (Robert and Kennett, 1992; Zachos et al., 2001; Pagani et al., 2005; Foreman et al., 2012; Huber and Goldner, 2012).

The development of Asian monsoon system during the Eocene period, which controls precipitation over mainland Asia, has been demonstrated (Liche et al., 2014; Huber and Goldner, 2012; Quan et al., 2012; Wang et al., 2013). Monsoon or monsoon-like climates have

prevailed over East Asia during the Paleogene (Quan et al., 2014). Quantitative Eocene climate studies have shown that the mean annual precipitations over China was more than 730 mm, indicating a sub-humid to humid climate in the Eocene period (Tong et al., 2002; Quan et al., 2012, 2014). The developments of coal and oil shale in the East China during the Eocene are also indicative for humid climate (Quan et al., 2014). The precipitation/evaporation balance in the East Asia during Middle Eocene was coupled to temperature change (Liche et al., 2014; Quan et al., 2014). High temperature commonly accompanied by high precipitation and strong weathering condition.

5.4. Mechanisms of TOC enrichment

Organic-rich marlstone, an attractive unconventional petroleum exploration target, was widely distributed in the Es₃¹ unit of the Shulu Sag, especially in Stage 3. Stage 3, corresponding to the MECO, likely had a mostly warm and humid climate during the deposition of Es₃¹. The warm and humid climate could have favored the formation of abundant precipitation and runoff, which led to increased export of dissolved carbonate and nutrient loads from surrounding provenance areas to the basin. Thus, primary productivity was likely the highest during Stage 3 due to the suitable environment and rich nutrients. During the period of Es₃¹ deposition, the relative lake level obviously rises and the lake basin was overall rapidly subsiding because of the temperature increase in MECO and the activity of the Xinhé fault, which is the boundary fault controlling the sag (Jiang et al., 2007). The subsidence of the basin floor along with the warm humid climate could create abundant accommodation space and form a deep lake with anoxic bottom water and low terrigenous clastic material input. Thus, the high primary productivity, anoxic deep lake environment with low terrigenous clastic material input formed widely distributed organic-rich marlstone with high TOC values in the sag, making the lower unit of the third member of the Eocene Shahejie Formation (Es₃¹) one of the most important petroleum exploration targets in the Bohai Bay Basin.

6. Conclusions

The deposits in the Es₃¹ unit of the Shulu Sag are carbonate mineral-rich and show strong heterogeneities. On the basis of the variation trend of the facies associations and the organic geochemical characteristics, Es₃¹ can be divided into 6 stages: shallow lake (Stage 1), rising lake (Stage 2), deep, freshwater lake (Stage 3), highly turbulent lake (Stage 4), stable lake (Stage 5), and turbulent lake (Stage 6). Combining the results of ATS and the radiometric age, the correlation between the evolutionary lake stages of Es₃¹ and the Eocene global climate curve was illustrated.

During Stage 1, which is the beginning of lake evolution, tectonic movement caused the subsidence of the basin and resulted in lake formation. The Stage 2 deposits indicate an upward trend of lake deepening, which was controlled by the increasingly warm and humid climate. The deposition in Stage 3 was influenced by the warm and humid climate during the thermal maximum period (MECO), forming a deep, freshwater lake. Stage 4 was influenced by both the cooling climate and intensive tectonic activity, resulting in a highly turbulent lake. Stage 5, stable lake, was mainly controlled by the slightly warming climate since the tectonic movement was relatively stable. Stage 6 was influenced by both the cooling climate and tectonic activity. The results show that the global mid-Eocene climate played an important role on the relative lake level changes and TOC enrichment. The MECO influenced the Es₃¹ become organic-rich strata and one of the most important petroleum exploration targets in the Bohai Bay Basin.

CRedit authorship contribution statement

Qing Li: Writing – original draft, Funding acquisition, Conceptualization. **Xuelian You:** Methodology, Funding acquisition. **Zaixing**

Jiang: Project administration, Formal analysis. **Shenghe Wu:** Investigation, Formal analysis. **Dali Yue:** Software, Data curation. **Jiangshan Li:** Visualization, Software. **Yuan Zhou:** Visualization, Software.

Declaration of competing interest

The authors declare that they have no known competing financial interests or personal relationships that could have appeared to influence the work reported in this paper.

Data availability

Data will be made available on request.

Acknowledgments

This study was financially supported by the National Natural Science Foundation of China (Grant No. 42372146 and 41972107). We are grateful to the PetroChina Huabei oil field for providing research funding, data access and for permission to publish.

References

- Abouelresh, M.O., Slatt, R.M., 2012. Lithofacies and sequence stratigraphy of the Barnett shale in east-central Fort Worth basin, Texas. AAPG (Am. Assoc. Pet. Geol.) Bull. 96, 34–43.
- Adegoke, A.K., Abdullah, W.H., Hakimi, M.H., Sarki Yandoka, B.M., 2014. Geochemical characterisation of Fika formation in the Chad (Bornu) Basin, northeastern Nigeria: implications for depositional environment and tectonic setting. Appl. Geochem. 43, 1–12.
- Bohacs, K.M., Grabowski, G.J., Carroll, A.R., Miskell-Gerhardt, K., 2007. Lithofacies architecture and sequence stratigraphy of the green river formation, greater green river basin, Wyoming and Colorado. Mt. Geol. 44, 39–60.
- Bohacs, K.M., 2012. Relation of hydrocarbon reservoir potential to lake-basin type: an integrated approach to unraveling complex genetic relations among fluvial, lake-plain, lake margin, and lake center strata. In: Baganz, O.W., Bartov, Y., Bohacs, K., Nummedal, D. (Eds.), Lacustrine Sandstone Reservoirs and Hydrocarbon Systems, vol. 95. AAPG Memoir, pp. 13–56.
- Bohacs, K.M., Carroll, A.R., Neal, J.E., Mankiewicz, P.J., 2000. Lake basin type, source potential, and hydrocarbon character: an integrated sequence-stratigraphic-geochemical framework. In: Gierlowski-Kordesch, E.H., Kelts, K.R. (Eds.), Lake Basins through Space and Time, AAPG Studies in Geology, vol. 46, pp. 3–33.
- Bougeois, L., Dupont-Nivet, G., de Rafélis, M., Tindall, J.C., Proust, J.N., Reichert, G.J., de Nooijer, L.J., Guo, Z., Ormukov, C., 2018. Asian monsoons and aridification response to Paleogene sea retreat and Neogene westerly shielding indicated by seasonality in paratethys oysters. Earth Planet Sci. Lett. 485, 99–110.
- Carroll, A.R., Bohacs, K.M., 1999. Stratigraphic classification of ancient lakes: balancing tectonic and climatic controls. Geology 27, 99–102.
- Carroll, A.R., Bohacs, K.M., 2001. Lake-type controls on petroleum source rock potential in nonmarine basin. AAPG (Am. Assoc. Pet. Geol.) Bull. 85, 1033–1053.
- Carroll, A.R., Bohacs, K.M., 1995. A Stratigraphic Classification of Lake Types and Hydrocarbon Source Potential: Balancing Climatic and Tectonic Controls: First International Limno-Geological Congress, Abstract Volume, pp. 18–19.
- Chen, J., Bi, Y., Zhang, J., Li, S., 1996. Oil-source correlation in the Fulin basin, Shengli petroleum province, East China. Org. Geochem. 24, 931–940.
- Duan, Y., Ma, L.H., 2001. Lipid geochemistry in a sediment core from ruogai marsh deposit, eastern qinghai-tibet plateau, China. Org. Geochem. 32, 1429–1442.
- Espitalié, J., Madec, M., Tissot, B., Mennig, J., Leplat, P., 1977. Source rock characterization method for petroleum exploration. Offshore Technology Conference, Houston, Texas, May 2–5, 1977, SPE Paper 2935, 6.
- Feng, Y., Jiang, S., Hu, S., Li, S., Lin, C., Xie, X., 2016. Sequence stratigraphy and importance of syndepositional structural slope-break for architecture of paleogene syn-rift lacustrine strata, Bohai Bay Basin, E. China. Mar. Petrol. Geol. 69, 183–204.
- Ficken, K.J., Li, B., Swain, D.L., Eglinton, G., 2000. A n-alkane proxy for the sedimentary input of submerged/floating freshwater aquatic macrophytes. Org. Geochem. 31, 745–749.
- Fiet, N., Quidelleur, X., Parize, O., Bulot, L.G., Gillot, P.Y., 2006. Lower Cretaceous stage durations combining radiometric data and orbital chronology: towards a more stable relative time scale. Earth Planet Sci. Lett. 246, 407–417.
- Flügel, E., 2004. Microfacies of Carbonate Rocks: Analysis, Interpretation, and Application. Springer, New York, p. 976.
- Foreman, B.Z., Heller, P.L., Clementz, M.T., 2012. Fluvial response to abrupt global warming at the Palaeocene/Eocene boundary. Nature 491 (7422), 92–95.
- Galazzo, F.B., Giusberti, L., Luciani, V., Thomas, E., 2013. Palaeoenvironmental changes during the middle Eocene Climatic Optimum (MECO) and its aftermath: the benthic foraminiferal record from the alano section (NE Italy). Palaeogeogr. Palaeoclimatol. Palaeoecol. 378, 22–35.

- Gierlowski-Kordesch, E.H., 1998. Carbonate deposition in an ephemeral siliciclastic alluvial system: jurassic shuttle meadow formation, newark supergroup, hartford basin, USA. *Palaeogeogr. Palaeoclimatol. Palaeoecol.* 140, 161–184.
- Gierlowski-Kordesch, E.H., 2010. Lacustrine carbonates. In: Alonso-Zarza, A.M., Tanner, L.H. (Eds.), *Carbonates in Continental Settings: Facies, Environments, Processes: Developments in Sedimentology*, vol. 61. Elsevier, Amsterdam, pp. 1–101.
- Goncalves, F.T.T., 2002. Organic and isotope geochemistry of the Early Cretaceous rift sequence in the Camamu Basin, Brazil: paleolimnological inferences and source rock models. *Org. Geochem.* 33, 67–80.
- Grygar, T.M., Hošek, M., Mach, K., Schnabl, P., Martinez, M., 2017. Climatic instability before the miocene climatic optimum reflected in a central European lacustrine record from the most basin in the Czech republic. *Palaeogeogr. Palaeoclimatol. Palaeoecol.* 485, 930–945.
- Hao, F., Zhou, X., Zhu, Y., Yang, Y., 2011. Lacustrine source rock deposition in response to co-evolution of environments and organisms controlled by tectonic subsidence and climate, Bohai Bay Basin, China. *Org. Geochem.* 42, 323–339.
- Hickey, J.J., Bo, H., 2007. Lithofacies summary of the mississippian barnett shale, Mitchell 2 T.P. Sims well, wise county, Texas. *AAPG (Am. Assoc. Pet. Geol.) Bull.* 91, 437–443.
- Hinnov, L.A., 2000. New perspectives on orbitally forced stratigraphy. *Annu. Rev. Earth Planet Sci.* 28, 419–475.
- Hinnov, L.A., 2004. Earth's orbital parameters and cycle stratigraphy. In: Gradstein, F.M., Ogg, J.G., Smith, A.G. (Eds.), *A Geologic Time Scale 2004*. Cambridge University Press, pp. 55–62.
- Hinnov, L.A., Ogg, J.G., 2007. Cyclostratigraphy and the astronomical time scale. *Stratigraphy* 4, 239–251.
- Hossain, H.M.Z., Sampei, Y., Roser, B.P., 2009. Characterization of organic matter and depositional environment of Tertiary mudstones from the Sylhet Basin, Bangladesh. *Org. Geochem.* 40, 743–754.
- Hou, Dujie, 2011. Oil and Gas Geochemistry. Petroleum industry press, Beijing, p. 414p.
- Huber, M., Goldner, A., 2012. Eocene monsoons. *J. Asian Earth Sci.* 44, 3–23.
- Jiang, Z., Chen, D., Qiu, L., Liang, H., Jun, M.A., 2007. Source-controlled carbonates in a small eocene half-graben lake basin (Shulu sag) in central Hebei province, North China. *Sedimentology* 54, 265–292.
- Jin, F.M., Han, C.Y., Wang, J.M., Guo, Y.J., Gao, Z.H., 2008. Application of organic geochemical parameters in sequence classification and correlation: a case study from lower Es₃ in Shulu sag, Jizhong depression. *Acta Sedimentol. Sin.* 26, 86–91 (in Chinese with English abstract).
- Jovane, L., Florindo, F., Coccioni, R., Dinarès-Turell, J., Marsili, A., Monechi, S., Roberts, A.P., Sprovieri, M., 2007. The middle Eocene climatic optimum event in the Contessa Highway section, Umbrian Apennines, Italy. *Geol. Soc. Am. Bull.* 119, 413–427.
- Laskar, J., Robutel, P., Joutel, F., Gastineau, M., Correia, A.C.M., Levrard, B., 2004. A long-term numerical solution for the insolation quantities of the Earth. *Astron. Astrophys.* 428, 261–285.
- Laskar, J., Fienga, A., Gastineau, M., Manche, H., 2011. La2010: a new orbital solution for the long-term motion of the Earth. *Astron. Astrophys.* 532 (17), A89.
- Li, M.S., Hinnov, L., Kump, L., 2019. Acycle: time-series analysis software for paleoclimate research and education. *Comput. Geosci.* 127, 12–22.
- Li, Q., Wu, S., Xia, D., et al., 2020a. Major and trace element geochemistry of the lacustrine organic-rich shales from the Upper Triassic Chang 7 Member in the southwestern Ordos Basin, China: implications for paleoenvironment and organic matter accumulation. *Mar. Petrol. Geol.* 111, 852–867.
- Li, Q., Jiang, Z., Liu, K., Zhang, C., You, X., 2014. Factors controlling reservoir properties and hydrocarbon accumulation of lacustrine deep-water turbidites in the Huimin depression, Bohai Bay Basin, East China. *Mar. Petrol. Geol.* 57, 327–344.
- Li, Q., You, X., Jiang, Z., Wu, S., et al., 2020b. Lithofacies and reservoir characterization of a source-controlled carbonate succession in a lacustrine rift basin, the Shulu Sag of Bohai Bay Basin, East China. *J. Petrol. Sci. Eng.* 192, 107180.
- Li, Q., You, X., Jiang, Z., Zhao, X., Zhang, R., 2017. A type of continuous petroleum accumulation system in the Shulu sag, Bohai Bay basin, eastern China. *AAPG (Am. Assoc. Pet. Geol.) Bull.* 101, 1791–1811.
- Liang, C., Jiang, Z., Cao, Y., Jing, W., Wang, Y., Fang, H., 2017. Sedimentary characteristics and origin of lacustrine organic-rich shale in the salinized Eocene Dongying Depression. *Geol. Soc. Am. Bull.* 130, 154–174.
- Liche, A., van Cappelle, M., Abels, H.A., et al., 2014. Asian monsoons in a late Eocene greenhouse world. *Nature* 513 (7519), 501–506.
- Meléndez, N., Liesa, C.L., Soria, A.R., Meléndez, A., 2009. Lacustrine system evolution during early rifting: el Castellar formation (Galve sub-basin, central Iberian chain). *Sediment. Geol.* 222, 64–77.
- Milankovitch, M., 1941. Kano der Erdbestrahlung und seine Anwendung auf das Eiszeitenproblem. *Academic Serbe* 133, 1–633.
- Mitchell, R.N., Bice, D.M., Montanari, A., Cleaveland, L.C., Christianson, K.T., Coccioni, R., Hinnov, L.A., 2008. Oceanic anoxic cycles? Orbital prelude to the Bonarelli Level (OAE 2). *Earth Planet Sci. Lett.* 267, 1–16.
- Mohialdeen, I.M.J., Hakimi, M.H., Al-Beyati, F.M., 2015. Biomarker characteristics of certain crude oils and the oil-source rock correlation for the Kurdistan oilfields, Northern Iraq. *Arabian J. Geosci.* 8, 1–17.
- Mukhopadhyay, P.K., Wade, J.A., Kruger, M.A., 1995. Organic facies and maturation of Jurassic/Cretaceous rocks and possible oil-source rock correlation based on pyrolysis of asphaltenes Scotian Basin Canada. *Org. Geochem.* 22 (1), 85–104.
- Ogawa, Y., Takahashi, K., Yamanaka, T., Onodera, J., 2009. Significance of euxinic condition in the middle Eocene paleo-Arctic basin: a geochemical study on the IODP Arctic Coring Expedition 302 sediments. *Earth Planet Sci. Lett.* 285, 190–197.
- Olsen, P.E., Kent, D.V., 1999. Long-period Milankovitch cycles from the late triassic and early jurassic of eastern north America and their implications for the calibration of the early mesozoic time-scale and the long-term behaviour of the planets: philosophical transactions. *Math. Phys. Eng. Sci.* 357, 1761–1786.
- Pagani, M., Zachos, J., Freeman, K., Tipple, B., Bohaty, S., 2005. Marked decline in atmospheric carbon dioxide concentrations during the Paleogene. *Science* 309, 600–603.
- Peters, K.E., Walters, C.C., Moldowan, J.M., 2005. *The Biomarker Guide*. Cambridge University Press, Cambridge, United Kingdom, p. 1155.
- Platt, N.H., Wright, V.P., 1992. Palustrine carbonates and the Florida everglades: towards an exposure index for the fresh-water environment? *J. Sediment. Petrol.* 62, 1058–1071.
- Prell, W., Kutzbach, J., 1992. Sensitivity of the Indian Monsoon to forcing parameters and implications for its evolution. *Nature* 360, 647–652.
- Prokoph, A., Agterberg, F.P., 2000. Wavelet analysis of well-logging data from oil source rock, Egret Member, offshore eastern Canada. *AAPG (Am. Assoc. Pet. Geol.) Bull.* 84, 1617–1632.
- Quan, C., Liu, Y.S., Utescher, T., 2012. Eocene monsoon prevalence over China: a paleobotanical perspective. *Palaeogeogr. Palaeoclimatol. Palaeoecol.* 365–366, 302–311.
- Quan, C., Liu, Z., Utescher, T., Jin, J., Shu, J., Li, Y., Liu, Y., 2014. Revisiting the Paleogene climate pattern of East Asia: a synthetic review. *Earth Sci. Rev.* 139, 213–230.
- Rein, B., Negendank, J.F.W., 1993. Organic Carbon Contents of Sediments from Lake Schalkenmehrener Maar: A Paleoclimate Indicator: Paleolimnology of European Maar Lakes. Springer, Berlin Heidelberg, pp. 163–171.
- Robert, C., Kennett, J.P., 1992. Paleocene and Eocene kaolinite distribution in the south Atlantic and southern ocean: antarctic climatic and paleoceanographic implications. *Mar. Geol.* 103 (1–3), 99–110.
- Rohl, U., Brinkhuis, H., Stickley, C., Fuller, M.D., Schellenberg, S.A., Wefer, G., Williams, G.L., 2004. Sea level and astronomically induced environmental changes in middle and late Eocene sediments from the East Tasman Plateau. In: Exon, N.F., Kennett, J.P., Malone, M. (Eds.), *The Cenozoic Southern Ocean: Tectonics, Sedimentation, and Climate Change between Australia and Antarctica*, vol. 151. American Geophysical Union (AGU), Geophysical Monograph Series, pp. 127–151.
- Sarg, J.F., Suriyamin, N., Tinavsuu-Milkeviciene, K., Humphrey, J.D., 2013. Lithofacies, stable isotopic composition, and stratigraphic evolution of microbial and associated carbonates, Green River Formation (Eocene), Piceance Basin, Colorado. *AAPG (Am. Assoc. Pet. Geol.) Bull.* 97, 1937–1966.
- Schulz, M., Mudelsee, M., 2002. REDFIT: estimating red-noise spectra directly from unevenly spaced paleoclimatic time series. *Comput. Geosci.* 28, 421–426.
- Serra, O., 1984. Fundamentals of well-log interpretation. In: Part 1: The Acquisition of Logging Data, 15A. Elsevier, Amsterdam, pp. 1–423. *Developments in Petroleum Science*.
- Tănăvsuu-Milkeviciene, K., Sarg, J.F., 2012. Evolution of an organic-rich lake basin – stratigraphy, climate and tectonics: piceance creek basin, eocene green river formation. *Sedimentology* 59, 1735–1768.
- Tanner, L.H., 2010. Continental carbonates as indicators of paleoclimate. *Dev. Sedimentol.* 62, 179–214.
- ten Haven, H.L., de Leeuw, J.W., Rullkötter, J., Sinninghe Damsté, J.S., 1987. Restricted utility of the pristane/phytane ratio as a paleoenvironmental indicator. *Nature* 330 (23), 641–643.
- Tissot, P.B., Welte, D.H., 1984. *Petroleum Formation and Occurrence 2nd*. Springer verlag, Berlin, p. 699.
- Tong, G.B., Liu, Z.M., Zheng, M.P., Yuan, H.R., Liu, J.Y., Wang, W.M., Li, Y.C., 2002. Primary study on quantitative reconstruction of middle-late Eocene climate in Jiangnan Basin. *Earth Sci. J. China Univ. Geosci.* 27, 357–363.
- Torrence, C., Compo, G.P., 1998. A practical guide to wavelet analysis. *Bull. Am. Meteorol. Soc.* 79, 61–78.
- Villa, G., Fioroni, C., Pea, L., Bohaty, S., Persico, D., 2008. Middle Eocene–late Oligocene climate variability: calcareous nannofossil response at Kerguelen plateau, site 748. *Mar. Micropaleontol.* 69 (2), 173–192.
- Wang, D., Lu, S., Han, S., Sun, X., Quan, C., 2013. Eocene prevalence of monsoon-like climate over eastern China reflected by hydrological dynamics. *J. Asian Earth Sci.* 62, 776–787.
- Wang, G., Lin, G., 2012. Eocene paleoclimate zone study in the Jiyang depression. *Bull. China Soc. Mineral Petrol. Geochem.* 31, 505–509 (In Chinese with English abstract).
- Wang, M., Wilkins, R.W.T., Song, G., Zhang, L., Xu, X., Li, Z., Chen, G., 2015. Geochemical and geological characteristics of the Es₃ lacustrine shale in the Bonan sag, Bohai Bay Basin, China. *Int. J. Coal Geol.* 138, 16–29.
- Weedon, G., 2003. *Time-Series Analysis and Cyclostratigraphy*. Cambridge University Press, Cambridge, pp. 1–259.
- Wu, H.C., Zhang, S.H., Jiang, G.Q., Huang, Q.H., 2009. The floating astronomical time scale for the terrestrial Late Cretaceous Qingshankou Formation from the Songliao Basin of Northeast China and its stratigraphic and paleoclimate implications. *Earth Planet Sci. Lett.* 278 (3–4), 308–323.
- Yang, M.H., Liu, C.Y., Yang, B.Y., 2001. Mesozoic tectonic transformation in Jizhong (central Hebei Province) Basin and its petroleum geological implications. *Geotect. Metallogenia* 25, 113–119 (in Chinese with English abstract).
- Yuan, G., Gluyas, J., Cao, Y., Oxtoby, N.H., Jia, Z., Wang, Y., Xi, K., Li, X., 2015. Diagenesis and reservoir quality evolution of the eocene sandstones in the northern dongying sag, Bohai Bay Basin, east China. *Mar. Petrol. Geol.* 62, 77–89.
- Zachos, J., Pagani, M., Sloan, L., Thomas, E., Billups, K., 2001. Trends, rhythms, and aberrations in global climate 65 ma to present. *Science* 292 (5517), 686–693.
- Zachos, J.C., Dickens, G.R., Zeebe, R.E., 2008. An early Cenozoic perspective on greenhouse warming and carbon-cycle dynamics. *Nature* 451, 279–283.

- Zhang, J., Jiang, Z., Gierlowski-Kordesch, E., Xian, B., Li, Z., Wang, S., Wang, X., 2017. A double-cycle lake basin formed in extensional to transtensional setting: the Paleogene Nanpu Sag, Bohai Bay Basin, China. *Sediment. Geol.* 349, 15–32.
- Zhao, X., Li, Q., Jiang, Z., Zhang, R., Li, H., 2014. Organic geochemistry and reservoir characterization of the organic matter-rich calcilutite in the Shulu sag, Bohai Bay Basin, north China. *Mar. Petrol. Geol.* 51, 239–255.
- Zheng, L., Jiang, Z., Liu, H., Kong, X., Li, H., Jiang, X., 2015. Core evidence of paleoseismic events in Paleogene deposits of the Shulu sag in the Bohai Bay Basin, East China, and their petroleum geologic significance. *Sediment. Geol.* 328, 33–54.